Particle Physics at CERN

Annual Report 2005

E. Alagöz, Y. Allkofer, C. Amsler, V. Boccone, A. Büchler, V. Chiochia,
S. Horikawa, C. Hörmann, I. Johnson, A. Knecht, K. Prokofiev, H. Pruys, C. Regenfus,
P. Robmann, J. Rochet, T. Speer, S. Steiner, D. Tsirigkas, and L. Wilke
Secretariat: P. Perréard

Physik-Institut der Universität Zürich
Winterthurerstrasse 190, CH-8057 Zürich, Switzerland

April 11, 2006

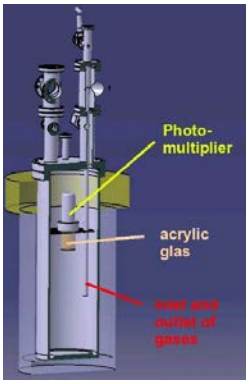

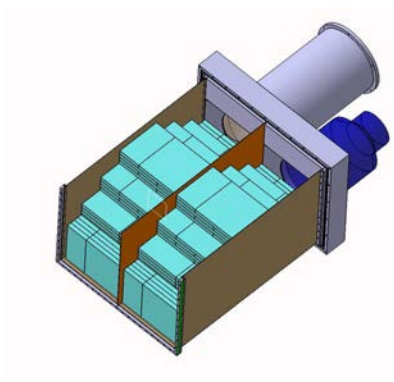

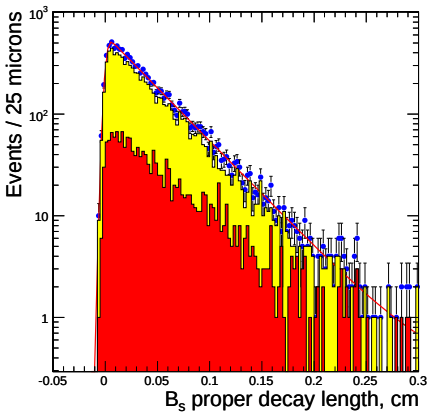

Contents

This report covers the activities of the Zurich group at CERN on the CMS, the DIRAC and the ArDM experiments between 1 April 2005 and 31 March 2006. It does not include the activity of C. Amsler within the Particle Data Group, contributing to the "Review of Particle Physics" . Further details on the group activities and publication reprints can be obtained from our home page (http://www.cern.ch/unizh/).

1 Particle physics with CMS

E. Alagöz, C. Amsler, V. Chiochia, C. Hörmann, K. Prokofiev[a], H. Pruys[b], C. Regenfus, P. Robmann, J. Rochet, T. Speer, S. Steiner, D. Tsirigkas[c], and L. Wilke

[a] until September 2005
[b] until August 2005
[c] CERN doctoral student

In collaboration with:
ETH - Zürich, Paul Scherrer Institut (PSI) and the CMS Collaboration

1.1 Summary

Physics at the LHC is the main activity of the Zurich group. We are interested in B-physics issues which can be performed during the first 2- 3 years of LHC operation, when the luminosity will still be too low for Higgs searches. In particular, we are preparing with the decay $B_s^0 \rightarrow (J/\psi)\phi \rightarrow \mu^+\mu^- K^+K^-$ a measurement of $B_s^0 - \bar{B}_s^0$ oscillations, of the lifetime of the CP-eigenstates B_s^H and B_s^L, and of CP-violation. Our group is contributing to the CMS reconstruction and simulation software using the pixel vertex detector required to efficiently tag B-decays. T. Speer has been appointed CMS coordinator for B - tagging. We are involved in the design, construction and test of the barrel pixel detector, a three layer cylindrical silicon device built mostly by Swiss institutions. We are responsible for performance measurements on test beams at CERN (such as position resolution, Lorentz angle and efficiency) on highly irradiated prototypes, and are leading the preparation of the online performance monitoring programs. V. Chiochia is coordinating the CMS pixel offline software group. We are also involved in the development of the sensor readout chip at PSI, and of the power distribution to the pixel detector. The mechanical support structure, cooling system and service tubes are built in the workshop of the Physik-Institut. Details on the software and detector performance can be found in the physics technical design report [1].

1.2 B - physics with CMS

The LHC will be commissioned in 2007 with an initial luminosity of about $10^{30} - 10^{33}$ cm^{-2}s^{-1}. An integrated luminosity of 30 fb^{-1} will be collected after three years of data-taking (assuming an overall beam and detector on efficiency of 30%), after which the luminosity will hopefully reach the design value of 10^{34} cm^{-2}s^{-1}. The main motivation for CMS is the search for the Higgs boson and for supersymmetric particles. However, unless the Higgs is heavy, a significant signal will not be observed during the first 2 - 3 years of operation at low luminosity. Meanwhile, our group intends to concentrate on issues related to the B_s-meson, making full use of the pixel vertex detector.

We intend to perform a high statistics study of the channel $B_s^0 \rightarrow (J/\psi)\phi$ with $J/\psi \rightarrow \mu^+\mu^-$ and $\phi \rightarrow K^+K^-$. This is a good channel to study many properties of B_s^0 - mesons, such as CP - violation, $B_s^0 - \bar{B}_s^0$ oscillations, and to measure the lifetimes of the two eigenstates, B_s^H and B_s^L. The pixel detector is an essential component for these studies requiring a precise determination of the mean life of the B_s^0-meson. Its relatively long lifetime (1.46 $\pm$ 0.06 ps) can be used to reject the short-lived background.

B_s^0 - $\bar{B}_s^0$ oscillations have not been observed so far since the oscillation frequency Δm_s is large. The lower limit (95% C.L.) on Δm_s is currently 14.4 ps^{-1} [2]. The relative difference between the mean lives of B_s^H and B_s^L is also predicted to be large, in the range 10 - 20%.

CP - violation and particle-antiparticle mixing can also be studied with $B_s^0 \rightarrow (J/\psi)\phi$. This decay proceeds mainly through the tree spectator diagram (fig. 1.1a), second order processes (such as penguin diagrams, fig. 1.1b) being suppressed.

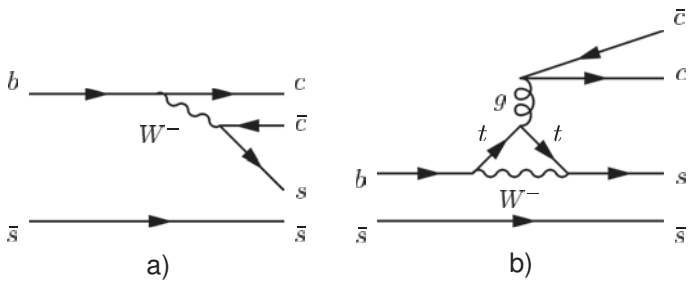

Figure 1.1: *Feynman diagram for the $B_s^0 \to (J/\psi)\phi$ decay (a). The penguin diagram (b) is suppressed.*

A full reconstruction of the B_s^0 is achieved through the decays $J/\psi \to \mu^+\mu^-$ and $\phi \to K^+K^-$. CP - violation is induced by interference between the decay and particle–antiparticle mixing. One measures the (CP - violating) asymmetry between $B_s^0 \to (J/\psi)\phi$ and $\bar{B}_s^0 \to (J/\psi)\phi$ which requires tagging the flavor of the B_s^0. An alternative method is to measure the angular distributions of the final state kaons and muons. The CP - even and CP - odd components correspond to even, respectively odd, relative angular momenta between the J/ψ and the ϕ, and have therefore different angular distributions [3]. This does not require tagging but very large data samples which can be obtained at the LHC. The decay rate asymmetry determines the CP - violating weak phase $\phi_{CKM} = 2\lambda^2\eta$, where $\lambda \equiv V_{us}$ and η is the height of the unitarity triangle, expected to be very small (about 0.03). The measurement of a significantly larger phase would indicate contributions from processes beyond the standard model.

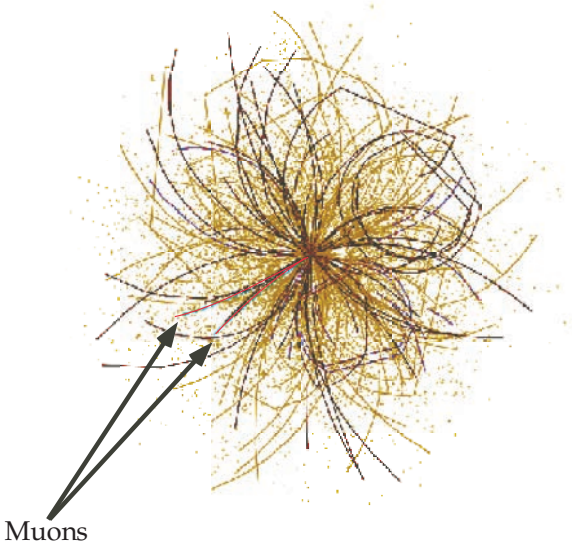

Figure 1.2: *A typical simulated event at CMS which contains a decay of the type $B_s^0 \to (J/\psi)\phi \to \mu^+\mu^-K^+K^-$.*

The branching fraction for $B_s^0 \to (J/\psi)\phi$ is about 10^{-3} [2]. With the help of simulations we have developed a selection strategy for the final state $K^+K^-\mu^+\mu^-$ relying on the reconstruction of the four charged particles by a high level trigger (HLT) [4]. An event of this type is shown in fig. 1.2. The muon trigger selects two muons of opposite charges from the muon chambers with a transverse momentum above 3 GeV/c. We require two muons tracks of opposite charges with mass within 100 MeV of the J/ψ mass, and two kaon tracks of opposite charges with mass within 100 MeV of the ϕ mass. The four tracks are required to come from a common secondary vertex. The trigger efficiency is about 10% [4].

Considerable progress was made in 2005 in the development of the tracking and vertex software

[5]. A general kinematic fitting program was developed for CMS [4]. The kinematic fit can be applied to $B_s \to (J/\psi)\phi \to K^+K^-\mu^+\mu^-$ during offline reconstruction to increase the experimental resolution on the B_s^0 mass which improves from 34 MeV to 14 MeV (fig. 1.3, left).

Some 250'000 signal events would be reconstructed after 2 years of LHC running with a background of about 40'000 events. For comparison, only a few hundred events have been observed so far for this decay channel. The resolution on the proper decay length ($c\tau_s$) of the B_s^0 meson is about 30 μm, from which one concludes that the observation of $B_s^0 - \bar{B}_s^0$ oscillations is possible with CMS, provided that the oscillation frequency is close to its present lower limit of $14.4\ \mathrm{ps}^{-1}$.

However, the lifetime difference between the two CP eigenstates B_s^H and B_s^L is too small to be measured directly. Figure 1.3 (right) shows a double exponential fit to the decay length distribution. This task will require an analysis of the angular correlations in the $K^+K^-\mu^+\mu^-$ final state which are different for B_s^H and B_s^L. A corresponding study is in progress. We are investigating in parallel the analogous decay $B_s \to (J/\psi)\ \phi$ where $J/\psi \to e^+e^-$. This decay will increase the B_s^0 sample, but the reconstruction of low-momentum electrons is notoriously difficult.

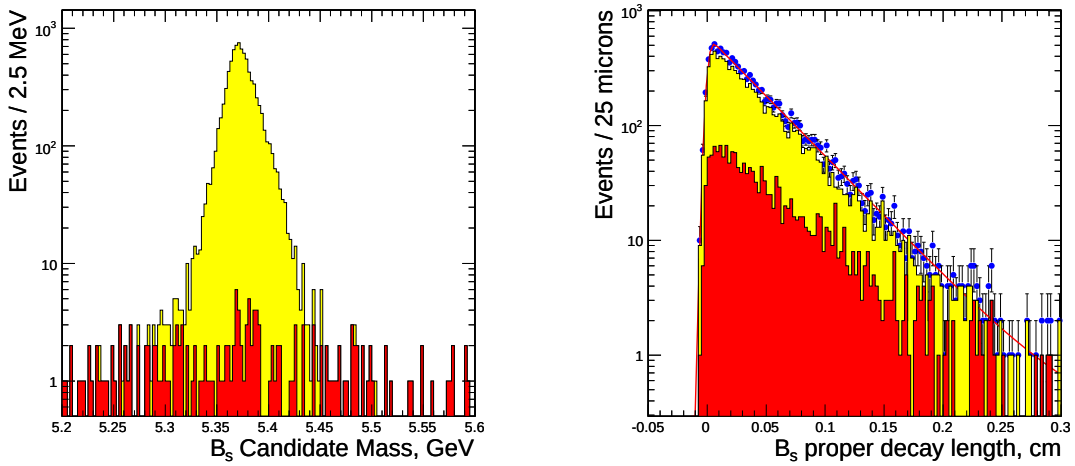

Figure 1.3: *Left: Invariant mass distribution of $B_s \to (J/\psi)\ \phi$ after the kinematics fit (yellow area). The bottom (red) area is the residual combinatorial background. Right: Distribution of decay length in the B_s rest frame showing the B_s^L contribution in yellow and the B_s^H contribution in red. The red curve is a two - component exponential fit (from ref. [4]).*

1.3 Silicon pixel sensors

The pixel detector consists of three concentric cylindrical layers, 53 cm long, with radii of 4.4, 7.3 and 10.2 cm, and forward/backward wheels. The pixel sensors are mounted on segmented silicon plates and are connected by indium bump bonds to the readout chips. The analog signals are read out using charge sharing between pixels to determine the coordinates more accurately. Details can be found in previous annual reports.

We have tested prototypes of sensors (pixel size $125 \times 125\ \mu\mathrm{m}^2$) with 105 - 225 GeV pions in the H2 beam line of the CERN SPS and measured the charge collection, hit detection efficiencies and the Lorentz angle [6, 7, 8, 9]. Oxygenated pixel sensors with p-spray isolation (manufactured by CiS, Erfurt) were chosen. The pixel cell size was finally fixed to $100 \times 150\ \mu\mathrm{m}^2$. Figure 1.4 shows a sketch of the final pixel cell layout.

In pixel sensors effects due to irradiation can be investigated with the grazing angle technique [8]. As shown in fig. 1.5 the surface of the sensor is tilted by a small angle (15°) with respect to the pion

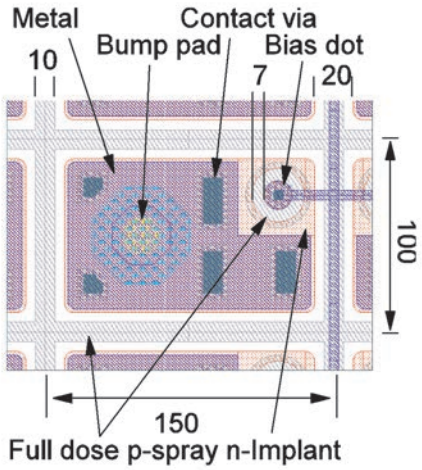

Figure 1.4: *Pixel cell layout for the barrel detector.*

beam. The charge measured by each pixel along the x direction samples a different depth z in the sensor. The precise entry point is measured with our silicon beam telescope which measures tracks with an r.m.s. position resolution of about 1 μm [10]. For unirradiated sensors the cluster length determines the depth over which charge is collected in the sensor.

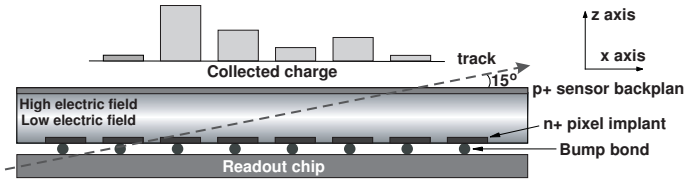

Figure 1.5: *Grazing angle method to determine the charge collection profiles.*

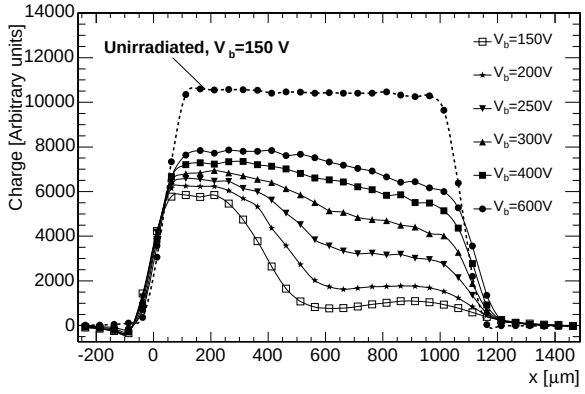

Figure 1.6: *Charge collection profiles measured with an unirradiated (dashed line) sensor and a sensor irradiated to* 6×10^{14} $n_{\mathrm{eq}}/\mathrm{cm}^2$ *(solid lines). The latter is operated at bias voltages* V_b *between 150 V and 600 V.*

The profiles measured with an unirradiated sensor and with a sensor irradiated to a fluence of 6×10^{14} $\mathrm{n_{eq}}/\mathrm{cm}^2$ are shown in fig. 1.6 as a function of the distance x from the beam entry point. This fluence corresponds to the first four years of LHC operation for the innermost layer. The unirradiated sensor was operated at a bias voltage of 150 V, well above its depletion voltage of 70 V). The irradiated sensor was operated at bias voltages between 150 V and 600 V. It appears to be partly depleted at 150 V, but a second peak is observed at large x. By increasing the bias voltage one also increases the amplitude of the second peak, as more charge is collected from the sensor side close to the backplane, while the increase at the n+ side is about 30%. At 600 V charge collection is saturated but the profile is not uniform due to the trapping of carriers produced far from the collecting electrode.

When a magnetic field is applied along the x-direction, the charge is deflected in the y-direction

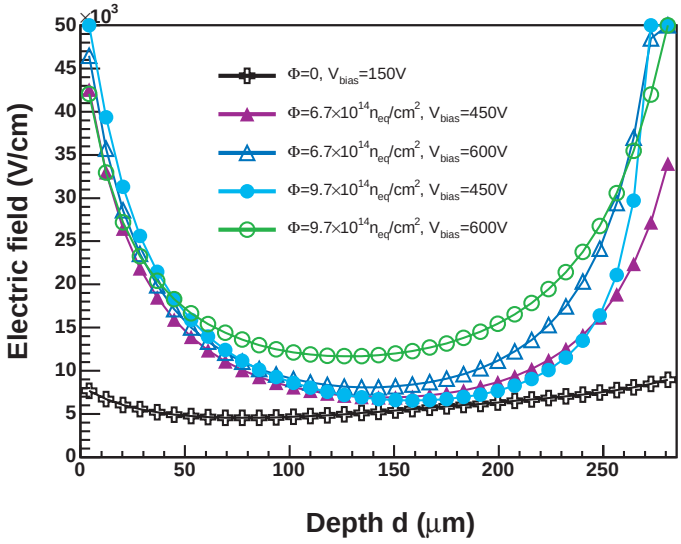

Figure 1.7: *Electric field as a function of sensor depth (from ref. [7]). The regions immediately below the surfaces ($\sim 20\mu$m) are affected by large systematic uncertainties (not shown).*

towards the adjacent pixel row. A measurement of the charge distribution among adjacent pixels yields the Lorentz angle θ_L as a function of x, and hence sensor depth. The Lorentz angle appears to depend on depth. A measurement of θ_L as a function of depth determines the behaviour of the electric field. Using a known empirical parametrization of the mobility one can extract the electric field as a function of sensor depth [7]. The electric field reaches maxima below both surfaces and a minimum in the bulk center (fig. 1.7). This behaviour in irradiated sensors does not correspond to the classical picture of a partially depleted sensor, but can be described by a double junction model [11].

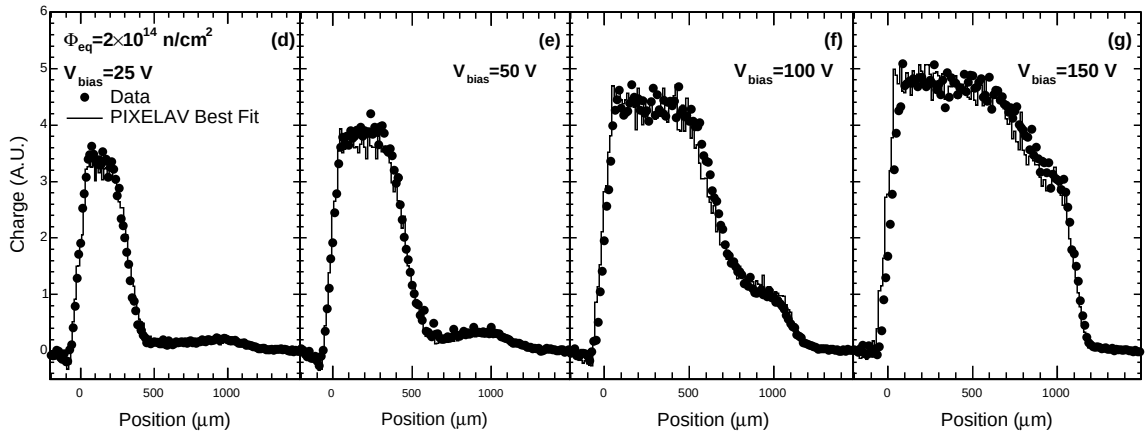

Figure 1.8: *Measured (dots) and simulated (histogram) charge collection profiles for a sensor irradiated to a fluence of 2×10^{14} $n_{\rm eq}/cm^2$ and operated at several bias voltages. The simulation was performed with the PIXELAV software (from ref. [11]).*

A detailed modeling (PIXELAV) of charge collection in heavily irradiated sensors was developed in collaboration with M. Swartz from Johns Hopkins University. This model takes into account e.g. the charge deposition by hadrons, a 3D intrapixel electric field map, the mobility, diffusion and trapping, and a simulation of the electronic noise [12]. Simulations were performed and tuned on the tests results described above for the 125×125 μm^2 sensors. The charge collection profiles for a sensor irradiated to a fluence of 2×10^{14} n$_{\rm eq}$/cm^2 and operated at several bias voltages are presented in fig. 1.8. The measured profiles are compared to the simulated PIXELAV profiles. The simulation describes the measured charge collection profiles rather well, both in shape and normalization. In

particular, the wiggle observed at low bias voltages is also described correctly.

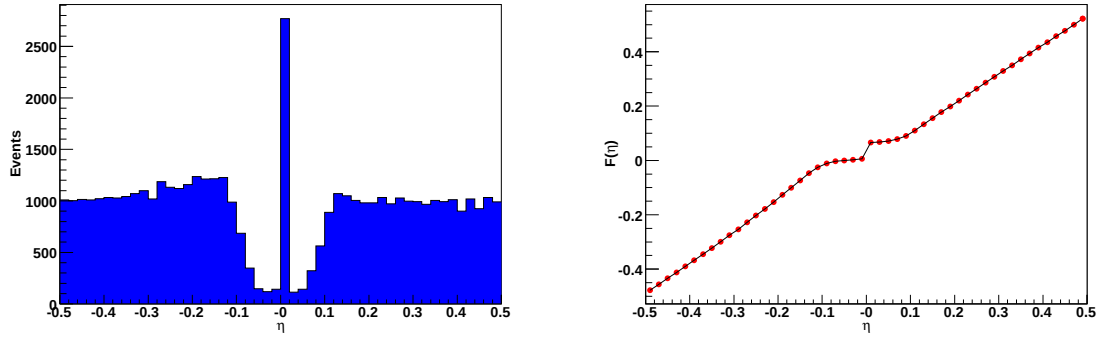

Figure 1.9: *a) Distribution of the reconstructed impact position within a single pixel for perpendicular tracks; b) Correction function $F(\eta)$ (from ref. [14]).*

Our simulations can now be applied to the final pixel dimensions of 100×150 μm^2. Since charge is shared among several pixels on can improve on the position resolution by applying the so - called η correction [13]. The hit position is first calculated with the center of gravity method. The η fraction is defined as the non - integer part of the reconstructed pixel number. Figure 1.9a shows the distribution of η for all events, where $\eta = 0$ corresponds to the center of the pixel cell and $\eta = \pm 0.5$ to the borders. The measured distribution is almost flat in the pixel regions close to the pixel borders but has a dip at the center. The peak at $\eta = 0$ is due to single pixel clusters. For each η one then associates a corrected value given by the function

$$F(\eta) = \frac{\int_{-0.5}^{\eta} \frac{dN}{d\eta}\, d\eta}{\int_{-0.5}^{0.5} \frac{dN}{d\eta}\, d\eta} - \frac{1}{2}, \tag{1.1}$$

where η is in pixel units. The $F(\eta)$ function is shown in fig. 1.9b. The corrected position is calculated by adding $F(\eta)$ to the integer part of the pixel number.

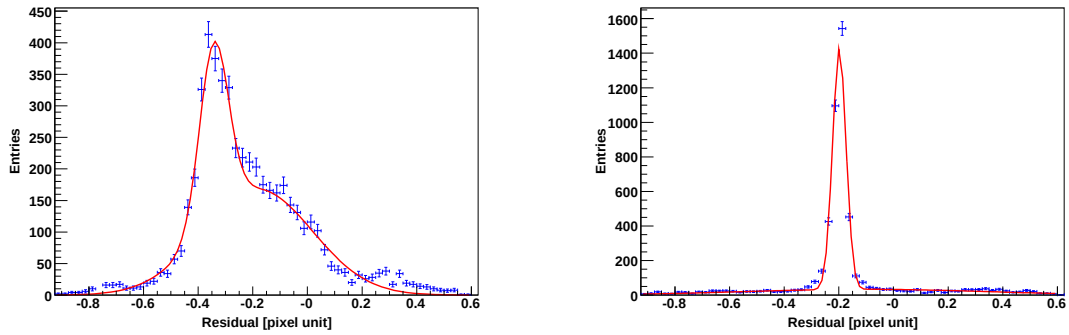

Figure 1.10: *Residual (simulated - reconstructed hit) distribution for tracks with an incident angle of 20°. The distributions are calculated without (left) and with η-corrections (right) and are not corrected for the Lorentz shift due to the magnetic field. The simulated data points are represented by markers and the continuous line is a double-Gaussian fit to the distribution (from ref. [14]).*

Figure 1.10 shows the residual distribution for clusters of two pixels, simulated for a sensor irradiated to 5.9×10^{14} n_{eq}/cm^2, and for tracks with an incident angle of $20°$ with respect to the normal to the sensor surface. The distribution before correction (left) is not described by a single Gaussian and is affected by large systematic errors which depend on the hit position. Systematic errors can be

largely reduced by applying the η-correction (fig. 1.10, right). This simulation shows that resolutions below 15 μm can be achieved after irradiation. A comparison with beam tests of the final sensors will be performed in 2006.

1.4 Readout electronics

We have also contributed to the readout chip (ROC), the design of which is under the direct responsibility of PSI. The ROC, manufactured in CMOS 0.25 μm technology by IBM, has a much higher yield (80%) than our previous prototype in DMILL radiation hard technology (20%). The first complete module (16 ROC chips, each reading 52 $\times$ 80 pixels) were irradiated with 300 MeV/c pions at PSI (fig. 1.11). The purpose was to measure the efficiency as a function of inclination ϕ and readout threshold, and to check the timing performance. The incoming intensity was typically 40 MHz/cm^2 (corresponding to the rate in the first pixel layer at 4.4 cm in LHC). The trigger was provided by two scintillators of dimensions $2 \times 2 \times 2$ mm^3 (which counted at a rate of 1 MHz) in coincidence with an americium radioactive source to simulate the level 1 trigger in CMS. The data analysis is in progress [15].

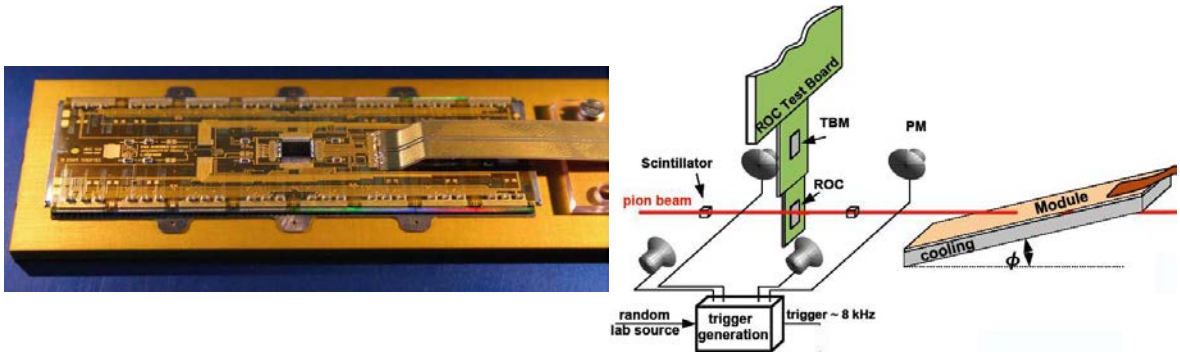

Figure 1.11: *Left: first assembled module consisting of 16 PSI46V2 readout chips bump-bonded to a sensor with 66'560 pixels. Right: setup for the beam tests at PSI.*

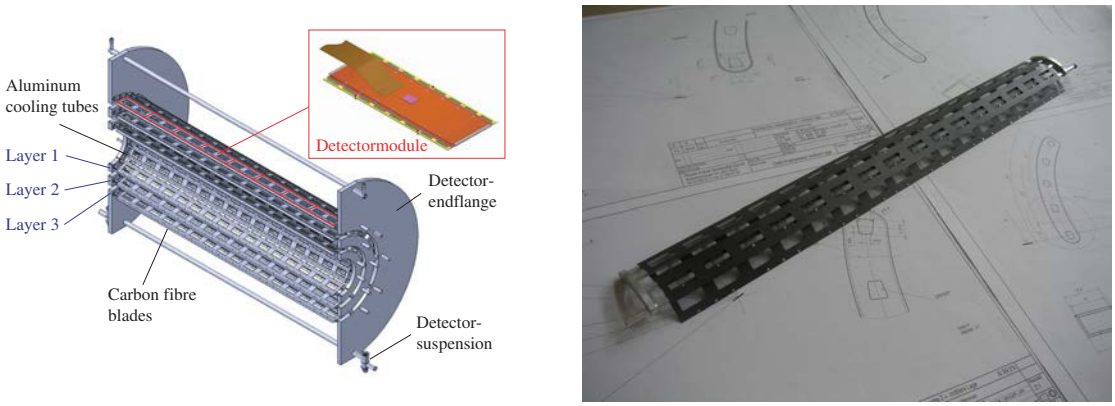

Figure 1.12: *Left: Half shell of the support structure with the three detector layers. Right: Prototype segment. The aluminum tubes are laser welded to the endflange containers that distribute the cooling fluid.*

1.5 Mechanical support structure

The Institute's workshop is building the support structure for the barrel pixel detector and the service tubes along the beam line. The pixel detector consists of three 57 cm long layers (fig. 1.12, left) equipped with silicon pixel modules and two 2.2 m long service tubes. Two vertically separated half shells will be introduced into the CMS detector.

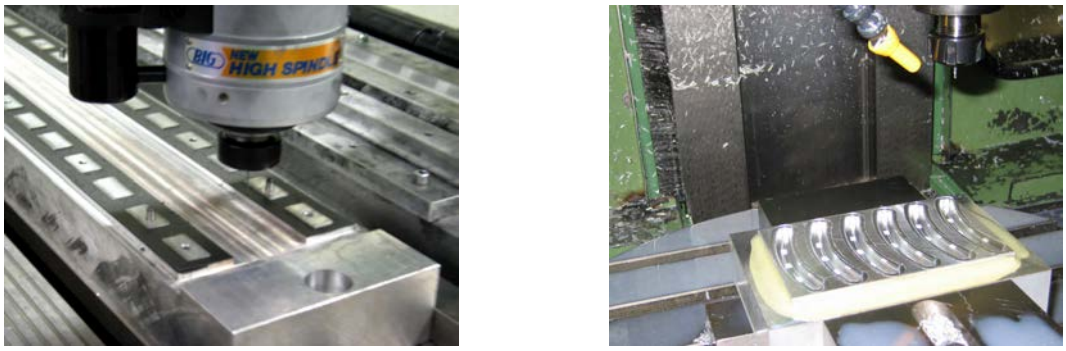

Figure 1.13: *Production of the carbon fiber blades (left) and of the cooling containers (right) on the milling machines of the Physik - Institut.*

The support structure consists of individual ladders built of pure aluminum tubes with trapezoidal cross sections and wall thickness of 300 μm. Custom made 240 μm thick carbon fiber blades which support the pixel modules are glued to the tubes, forming the detector segments (fig. 1.12, right). Four to five of these tubes are then laser welded to an aluminum container which distributes the coolant. The manifold provides the cooling of the detector modules to about -10°C with C_6F_{14}. Support frames on both ends connect the segments and form a detector layer half shell. The flanges consist of thin fiberglass frames (FR4) filled with foam (Airex) covered by carbon fiber blades. This technique guarantees stability and precision for a minimum mass. Mass production of the various components (blades, cooling containers, etc.) is performed in our workshop (fig. 1.13). The laser welding technique (in collaboration with industry) was strongly improved. We have upgraded the welding equipment to prevent leakage of the coolant and have obtained higher quality welding seams than achieved before.

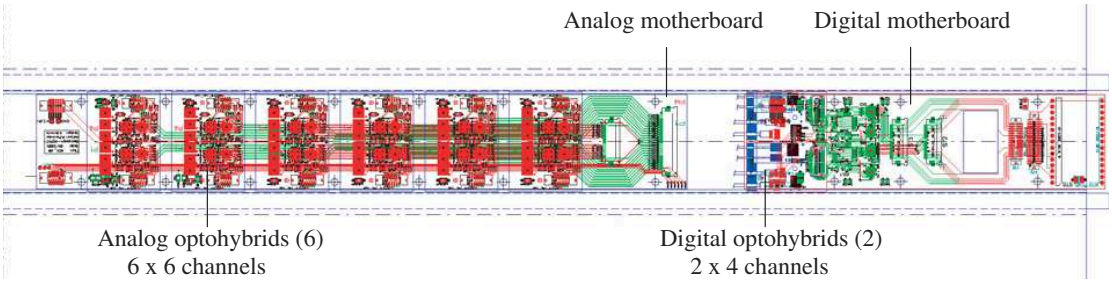

Figure 1.14: *Sketch of the readout slot with the analog and digital motherboards holding the optical hybrids.*

The electrical power, control and optical signals and the coolant are transferred to the detector through supply tubes. The forward and backward supply tubes are mechanically connected and carry the pixel detector. The structure is made of tubes and is filled with foam. The motherboards (fig. 1.14) holding the optical hybrids for analog and digital controls, will be installed near the detector. The outer ends contain power regulators and connectors for the electrical and optical lines, and the

central region the digital control boards and slow controls, such as voltages, currents, temperatures, pressures and humidity.

The project proceeds according to schedule. The 800 modules required for the three pixel layers will be assembled at PSI. In 2006 our group will perform further beam tests at CERN. Production of the parts for the three layers is proceeding in our workshop. Prototypes of the service tubes will be built in 2006. The pixel detector will be introduced into CMS after the LHC commissioning in 2007, to prevent damage during initial beam tuning. We are preparing a test support structure for the 2007 pilot run, consisting of a half shell partially equipped with detectors.

References

[1] E. Alagöz et al. CMS TDR I : Software and detector performance, CMS - TDR - 08, CERN-LHCC-2006-001

[2] S. Eidelman *et al.* (Particle Data Group), Phys. Lett. **B 592** (2004) 1

[3] A.S. Dighe *et al.*, Phys. Lett. **B 269** (1996) 144; Eur. J. Phys. **C6** (1999) 647

[4] K. Prokofiev, PhD Thesis, Universität Zürich (2005); K. Prokofiev Proc. 10th Int. Conf. on B-Physics at Hadron Machines (BEAUTY 2005), Assisi, Nucl. Phys. **B** Proc. Suppl. **156** (2006) 109

[5] T. Speer *et al.*, Proc. of the Workshop on Tracking in High Multiplicity Environments (TIME 2005), Zurich (in print); T. Speer and R. Frühwirth, Comp. Phys. Comm (in print)

[6] R. Kaufmann, PhD Thesis, Universität Zürich (2001)

[7] A. Dorokhov, PhD Thesis, Universität Zürich (2005); A. Dorokhov *et al.*, Proc. Vertex 2004 Conf., Como, 2004, Nucl. Instr. Meth. in Phys. Research **A** (in print), prep. physics/0412036

[8] A. Dorokhov *et al.*, Nucl. Instr. and Meth. in Phys. Research **A 530** (2004) 71

[9] T. Rohe *et al.*, Nucl. Instr. and Meth. in Phys. Research **A 552** (2005) 232

[10] C. Amsler *et al.*, Nucl. Instr. and Meth. in Phys. Research **A 480** (2002) 501

[11] V. Chiochia *et al.*, Proc. 2004 IEEE Trans. on Nucl. Sc. **52** (2004) 1067; V. Chiochia *et al.*, Proc. 10th Eur. Symp. on Semiconductor Detectors, Wildbad-Kreuth, Nucl. Instr. Meth. in Phys. Research **A** (in print), prep. physics/0506228

[12] M. Swartz, Nucl. Instr. and Meth. in Phys. Research **A 511** (2003) 88

[13] E. Belau *et al.*, Nucl. Instr. and Meth. **214** (1983) 253

[14] E. Alagöz, V. Chiochia, M. Swartz, Proc. of the Workshop on Tracking in High Multiplicity Environments (TIME 2005), Zurich, Nucl. Instr. Meth. in Phys. Research **A** (in print), prep. physics/0512027

[15] C. Hörmann, PhD Thesis, Universität Zürich, in preparation

2 Search for $K\pi$-atoms

Y. Allkofer, C. Amsler, S. Horikawa, I. Johnson[a], H. Pruys[b], C. Regenfus, and J. Rochet

[a] until October 2005
[b] until August 2005

In collaboration with:
Academy of Sciences of the Czech Republic, CERN, KEK (Tsukuba), Institute of Atomic Physics (Bucarest), JINR (Dubna), Laboratory Nazionali di Frascati, IHEP (Protvino), University of Basel, Bern, Ioannina, Kyoto, Lomonosov, Prague, Santiago, Trieste, Tokyo (Metropolitan)

(DIRAC II Collaboration)

2.1 The $K\pi$ scattering length

The $K^-\pi^+$-atom is a hydrogen-like non-relativistic system of a K^- and a π^+ bound by the Coulomb force. Such atoms have not been observed so far, in contrast to $\pi^+\pi^-$ atoms which were observed and studied by the DIRAC Collaboration at CERN [1]. For $K\pi$-atoms the binding energy of the 1s level is 2.9 keV and the Bohr radius 250 fm. The atom is unstable and decays into $\bar{K}^0\pi^0$ (fig. 2.1). The atomic level is shifted by the overlap of the pion and kaon wave functions. The energy shift, determined by the scattering lengths a_1 and a_3 in the isospin 1/2 and 3/2 $K\pi$ states, respectively, is predicted to be about - 10 eV (i.e. towards stronger binding) [2]. Up to a calculable small correction [2] the width Γ (or the lifetime τ) of the 1s level is related to the scattering lengths by the equation

$$\Gamma = \frac{1}{\tau} = 8p^*\mu^2\alpha^3 \left[\frac{a_1 - a_3}{3}\right]^2 , \tag{2.1}$$

where p^* = 11.5 MeV/c is the π^0 (or K^0) momentum in the rest frame of the atom, μ is the $K\pi$ reduced mass, and α the fine-structure constant.

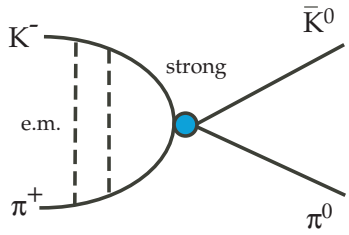

Figure 2.1: $K^-\pi^+$ - *atoms decay into* $\bar{K}^0\pi^0$.

Predictions for τ can, in principle, be derived from the $K\pi$ S - wave phase shifts obtained from $K\pi$ - scattering, e.g. by scattering kaons on nucleons (fig. 2.2, left). We recall that the scattering lengths a_1 and a_3 are the *slopes* of the phase shifts $\delta_1(k)$ and $\delta_3(k)$ in the limit where the momentum k becomes vanishingly small. The scattering lengths a_1 and a_3 are poorly known. Figures 2.2 a and 2.2 b show the S - wave $K\pi$ phase shifts from ref. [3]. The δ_1 ($S_{1/2}$) - phase is poorly known below 1 GeV, showing a peculiar oscillation pattern. Above 1 GeV the S - wave interaction is dominated by the $K_0^*(1430)$ resonance. Figures 2.2 b also shows the $P_{1/2}$ phase which is dominated by the $K^*(892)$ resonance.

The interaction is attractive in the i = 1/2 and repulsive in the i = 3/2 state. The uncertainties in a_1 and a_3 are substantial: the extrapolation to zero energy from the various phase shift measurements disagree by large factors: measurements of a_1 vary between 0.17 and 0.34 m_π^{-1}, those of a_3 between - 0.07 and - 0.14 m_π^{-1}. The scattering lengths were also computed from dispersion relations using scattering data, assuming analytical continuation, unitarity and crossing symmetry [4]:

$$a_1 = 0.224 \pm 0.022\ \mathrm{m}_\pi^{-1} \ \text{ and } \ a_3 = -0.0448 \pm 0.0077\ \mathrm{m}_\pi^{-1}, \tag{2.2}$$

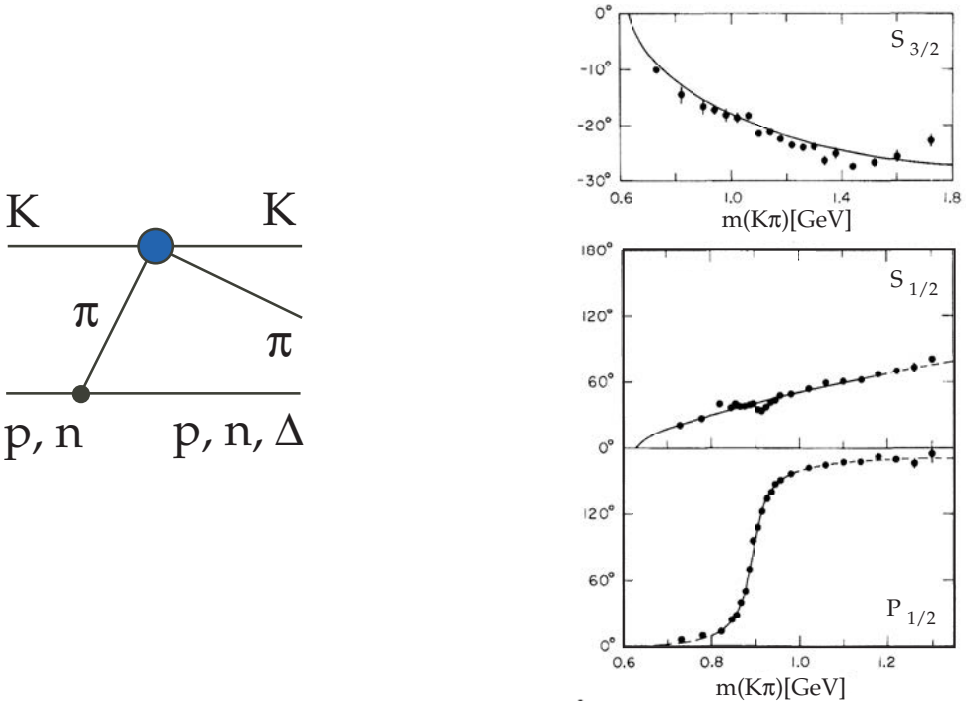

Figure 2.2: *Left: $K\pi$-scattering in Kp - interactions. Right: $K\pi$ phase shifts from ref. [3] showing the δ_3 ($S_{3/2}$), the δ_1 ($S_{1/2}$), and the $P_{1/2}$ phases as a function of $K\pi$ mass.*

However, there are inconsistencies below 1 GeV/c [4]. Using eqs. (2.1) and (2.2) one finds a mean life $\tau \sim 3.7$ fs for the $K\pi$ atom, with a rather large uncertainty.

The scattering lengths are of great importance for chiral perturbation theories (ChPT). The mean life of $\pi^+\pi^-$-atoms, recently measured by the DIRAC Collaboration [1], is in excellent agreement with predictions from ChPT [5] and with direct measurements of the scattering length from the $K \to \pi^+\pi^- e\nu$ decay [6]. In contrast, the $K\pi$ - scattering length probes ChPT extended to s-quarks, i.e. in the limit where the masses of the u-, d- and s-quarks vanish. Figure 2.3 shows the prediction for a_3 vs. a_1 from ChPT predictions [7], together with the dispersion calculation from ref. [4]. They are not in good agreement and there is a strong correlation between a_3 and a_1. The blue band shows the sensitivity of a hypothetical 20% accurate measurement of the lifetime of $K\pi$-atoms. A 20% measurement error in the lifetime leads to a 10% error in $|a_1 - a_3|$.

A measurement of the scattering length also yields information on nearby broad resonances. As mentioned above, S - wave $K\pi$ scattering is dominated by the $K_0^*(1430)$ resonance. However, there is mounting evidence for a very broad resonance around 800 MeV, the $K_0^*(800)$ (or κ). For example, recent data in $J/\psi \to K^+K^-\pi^+\pi^-$ report the κ at a mass of $\sim$ 800 MeV with a width of $\sim$ 600 MeV [8]. Establishing the κ is essential to understand the nature of scalar mesons. The ground state nonet could be made of the four-quark states and/or meson-meson resonances $a_0(980)$, $f_0(980)$, $f_0(600)$ (σ) and $K_0^*(800)$ (κ) [9]. If the latter indeed exists as a very broad state, it will influence the value of a_1.

2.2 The DIRAC II experiment

The Zurich group has joined the DIRAC experiment and will concentrate on the search and study of $K\pi$ - atoms. We will provide the aerogel Čerenkov counters for kaon detection and also the heavy

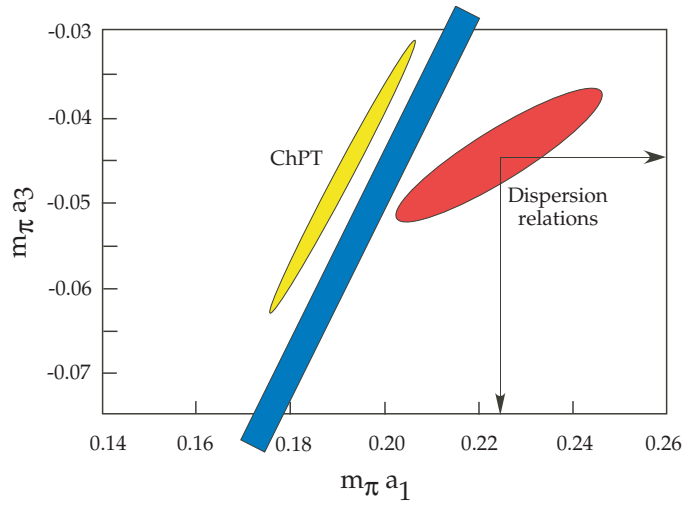

Figure 2.3: *a_3 vs. a_1 from ChPT [7] and from dispersion relations [4]. The most recent measurements ($m_\pi a_1$ = 0.335 $\pm$ 0.006, $m_\pi a_3$ = - 0.14 $\pm$ 0.007, see ref. [3]) lie outside the range of this plot. The blue band shows the sensitivity of a 20% measurement of the mean life of $K\pi$-atoms.*

gas system for the pion Čerenkov counters.

In the DIRAC apparatus kaons and pions are produced by the primary 24 GeV/c proton beam from the PS impinging on a 100 μm thick nickel foil [10]. The emerging particles are analyzed in a double-arm magnetic spectrometer measuring the momentum vectors of two oppositely charged hadrons (fig. 2.4). $K^-\pi^+$ - atoms, once produced, move forward and either annihilate into $\bar{K}^0\pi^0$ or ionize in the target. Since annihilation and ionization are competing processes, the mean life is obtained by measuring the breakup probability in the target, which can be calculated as a function of mean life. It is about 30 % in a 100 μm Ni target, assuming a mean life of 4.7 fs [11].

The breakup probability is given by the ratio of the number of dissociated pairs to the number of produced atoms. The dissociated kaon and pion emerge behind the target with a very small relative momentum $Q < 3$ MeV/c. One therefore expects an accumulation of events near $Q = 0$ which gives the number of dissociated pairs. Then one calculates the number of produced $K\pi$-atoms by measuring the number of unbound Coulomb pairs from the measured Q-distribution at large Q. The number of produced $K\pi$-atoms is obtained through a known relation between unbound and bound Coulomb pairs. This procedure has been applied to $\pi^+\pi^-$ atoms and details can be found in ref. [1].

The DIRAC apparatus (fig. 2.4) has to be modified to discriminate beween pions and kaons. Muons are identified by counters behind the concrete absorber. Electrons trigger the N_2 gas Čerenkov counter. The new C_4F_{10} gas Čerenkov counter identifies pions, while kaons are detected in the aerogel Čerenkov. Contaminating protons in the left arm are suppressed since they are below threshold for Čerenkov radiation. The right arm aerogel (for $K^-\pi^+$ - atoms) is not essential since the flux of antiprotons is much smaller than the flux of negative kaons.

2.3 The aerogel counters

Figure 2.5 shows the momentum distribution of kaons from $K\pi$-atoms at the entrance of the Čerenkov counters as a function of horizontal coordinate (in the plane of fig. 2.4). This distribution was calculated using the known production cross sections at 24 GeV/c. Kaons from $K\pi$-atoms have momenta between 3.9 and 8.9 GeV/c. Figure 2.5 also shows the vertical distribution which is not flat due to the slight upwards inclination of the spectrometers. For the emission of Čerenkov radiation the refractive index n has to be chosen so that $n > 1/\beta$ (where β is the velocity of the particle). Hence the quantity

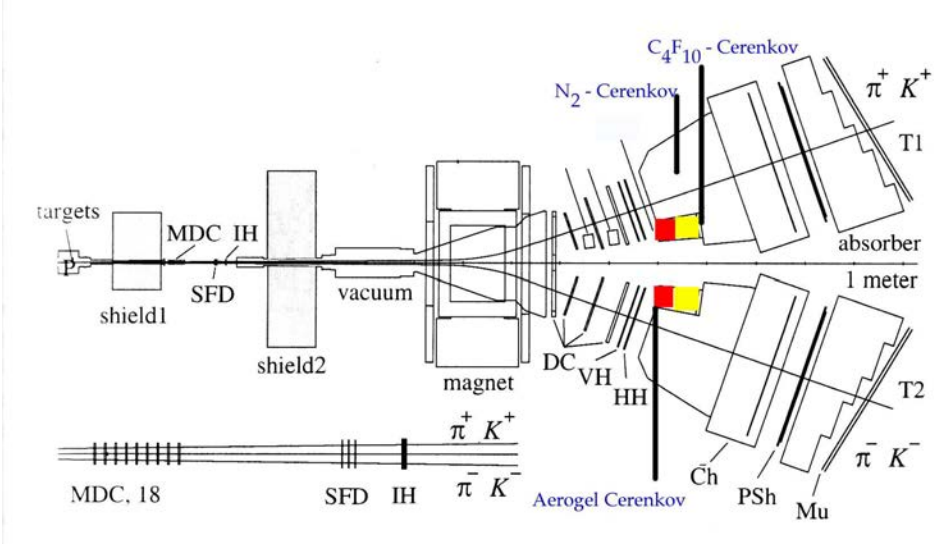

Figure 2.4: *Sketch of the updated DIRAC spectrometer, showing the locations of the Čerenkov counters to identify electrons, pions and kaons. MDC = microdrift chambers, SFD = scintillating fibre detector, IH = ionization hodoscope, DC = drift chambers, VH, HH = scintillation hodoscopes, PSh = preshower, Mu = muon counters.*

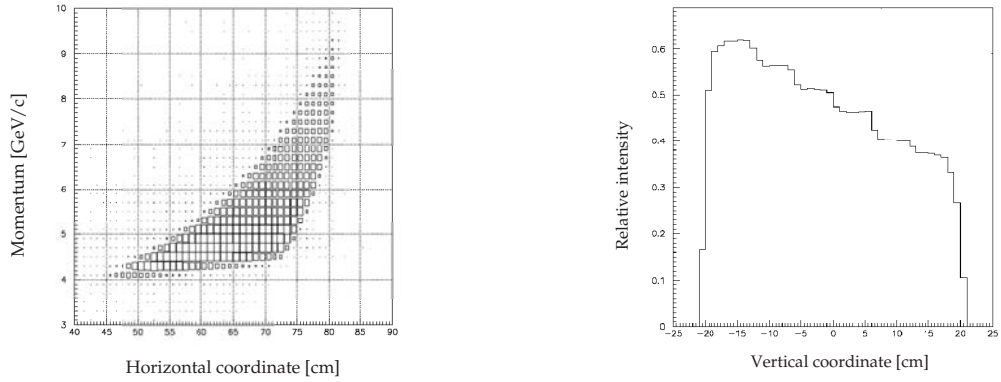

Figure 2.5: *Left: momentum distribution of kaons from the breakup of $K\pi$-atoms. Small angles with respect to the primary proton beam are towards the right. Right: vertical distribution.*

$n-1$ has to be small enough to avoid signals from fast protons ($\beta \simeq 1$), yet large enough to detect kaons. In the momentum range covered by the apparatus, n is required to be typically 1.010, which is larger than can be achieved with pressurized gas counters and smaller than for all known solid or liquid radiators, except aerogel. One concludes from fig. 2.5 that the aerogel counter has to cover a surface of about 35 x 40 cm^2.

Aerogel is made of colloidal SiO_2 grains of size $\sim$ 2 nm and pores $\sim$ 50 nm. The index of refraction depends on density ρ ($n = 1 + 0.21\rho$ [g/cm^3]). For example, for the $n = 1.008$ aerogel needed here, the density is 0.039 g/cm^3. The light yield is proportional to the factor

$$f = 1 - \frac{1}{\beta^2 n^2} \tag{2.3}$$

which decreases quickly when $n \simeq 1$. This fact is the main difficulty with thin Čerenkov counters. As we show below in fig. 2.7, a good $K-p$ separation can be achieved with two indices of refraction, n = 1.008 and 1.015. The lowest index is needed to improve the separation in the region of high energy

protons close to the primary beam line. The 1.015 counter is segmented into two parts to reduce pileup. Figure 2.6 shows the conceptual design. Each counter is vertical (40 cm long) viewed by two photomultipliers, one at each end.

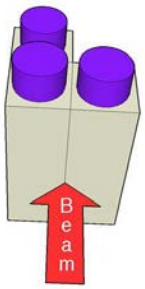

Figure 2.6: *Three aerogel counters are needed to separate protons from kaons. The upstream pair has n = 1.015, the downstream counter n = 1.008. Small angles with respect to the primary proton beam are towards the left.*

We have initiated an R&D programme to measure the light yield of aerogel and to optimize the geometry. Most of the measurements were made with n = 1.05 aerogel which is easily available. We have measured the number of photoelectrons $N_{p.e.}$ for a thickness of 10 cm of aerogel and for a 10 cm long slab viewed by two photomultipliers (PM) with UV windows. The measurements were made with cosmic ray muons which have an average momentum of 700 MeV/c ($\bar{\beta}$ = 0.989) since test beams were not available at CERN in 2005. We have obtained about 3 photoelectrons / cm of aerogel (summing the signals from both tubes). Extrapolation from n = 1.05 to lower indices and β = 1 can then easily be made using eq. (2.3).

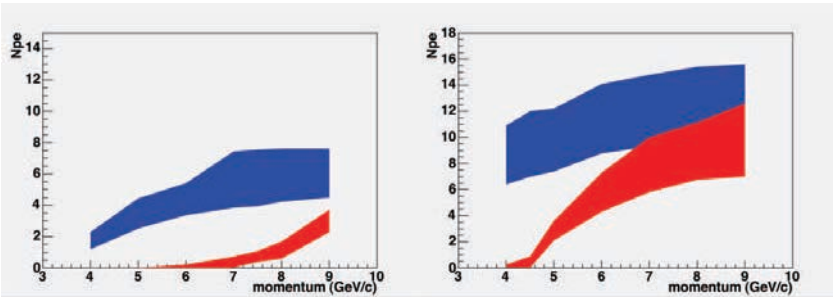

Figure 2.7: *Average number of photoelectrons as a function of momentum for n = 1.008 (left) and 1.016 (right) for a thickness of 15 cm and a length of 40 cm.*

However, the absorption length increases rapidly from about 10 cm at 270 nm to 3 m at 350 nm [12]. Therefore, 40 cm long aerogel counters are likely to be problematic. Figure 2.7 shows the expected average number of photoelectrons as a function of momentum for kaons and protons. The upper boundaries of the bands are for particles traversing the counter close to one of the PM, the lower boundary for those crossing the counter in the middle. The strong absorption can be compensated by increasing the thickness of aerogel in the middle of the counter (see fig. 2.11 below), which is easily feasible since aerogel is delivered in 1cm thick tiles. Figure 2.8 shows a simulation of the signal attenuation.

We also tried a novel setup using wavelength shifters (WLS). Figure 2.9 (left) shows the arrangement in our lab. The 2.5 cm thick aerogel tiles were sandwiched between reflective Tetratex foils which were sprayed with WLS. For example, p-terphenyl dissolved in chloroform shifts light from 270 to 340 nm, which reduces absorption and leads to some 5.5 p.e. /cm or 7 p.e. /cm for $\beta = 1$ (fig. 2.9, right). Using this last figure one then expects about 3 (12) photoelectrons at 4.5 (8) GeV/c for 15 cm of 1.008 aerogel. These results are quite encouraging when compared to fig. 2.7a, but they need to be checked with a prototype of the final length and depth.

We have also built a simple apparatus to measure the refractive index of aerogel using the refrac-

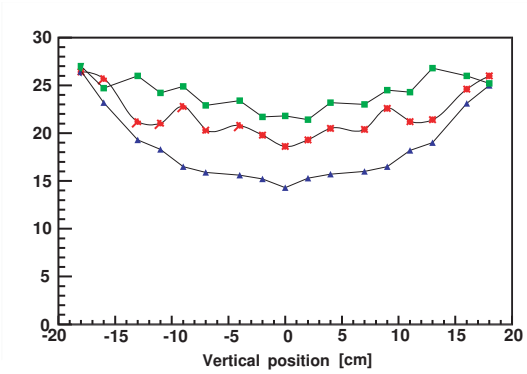

Figure 2.8: *Signal amplitude as a function of the distance at which the particle crosses the aerogel counter (arbitrary scale). The photomultipliers are located at the edges (± 20 cm). The blue (bottom) curve is for a counter with constant thickness, the red (middle) curve for 4 additional tiles and the green (top) curve for 6 additional tiles in the middle of the counter.*

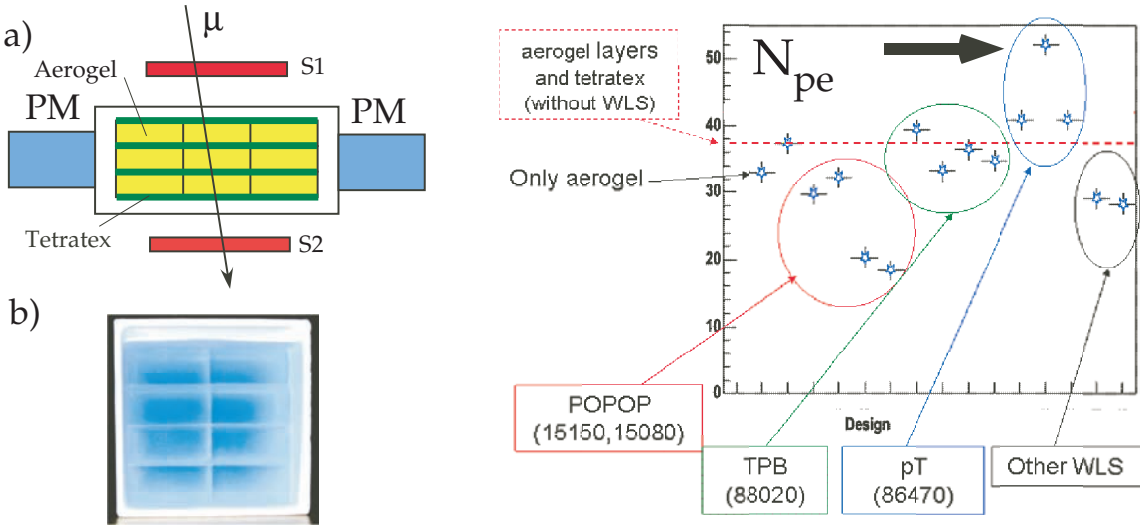

Figure 2.9: *Left: a) setup for light yield measurements, b) photograph of the aerogel tiles. Right: number of photoelectrons for a 10 cm thick, 10 cm long, n=1.05 aerogel counter, using cosmic muons, and for different geometries and WLS. The arrow shows the optimum design with p-terphenyl dissolved in chloroform.*

tion of a laser beam, following ref. [12]. Figure 2.10 shows a tile of aerogel illuminated by a laser beam incident under the angle α. One measures the displacement of the beam spot on a distant screen, i.e. the deflection γ of the beam which exits the aerogel:

$$\gamma = \alpha - \left[\beta + \frac{\pi}{2}\right] + \mathrm{asin}[\sin\alpha \sin\beta + n\sqrt{1 - \frac{\sin^2\alpha}{n^2}}\cos\beta]. \tag{2.4}$$

With at least two incident angles α one can eliminate β (expected to be around 0^0). Figure 2.10 shows the measurements for a piece of n = 1.05 aerogel, together with the fit leading to $n = 1.055 \pm 0.002$.

Figure 2.11 shows the design of the n = 1.015 aerogel detector built in the workshop of the Physik - Institut. The 5" Photonis - Philips XP4570/B photomultipliers with UV windows will be used. The 14 ℓ of n = 1.008 aerogel has been produced by the Budker and Boreskov Institutes in Novosibirsk, the 24 ℓ of n = 1.015 by Panasonic. The construction and tests are being performed in early 2006 and the detectors will be installed in the summer of 2006, when DIRAC resumes data taking. DIRAC (PS212) has been approved by the CERN Research Board to run at least until 2008. Extrapolating from $\pi\pi$ data, we estimate that some 1000 $K\pi$-atoms should be observed by DIRAC during 2006 - 2008.

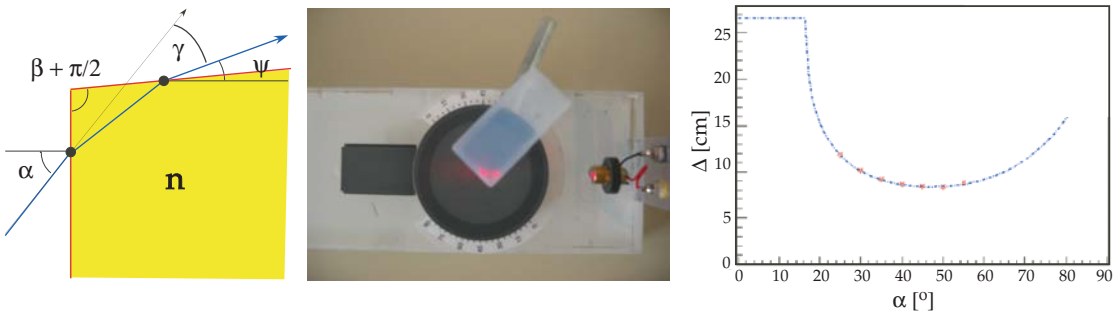

Figure 2.10: *Left: principle of setup to measure the refractive index. Middle: photograph of the setup. Right: measurement of laser spot displacement as a function of incident angle, with fit following eq. (2.4).*

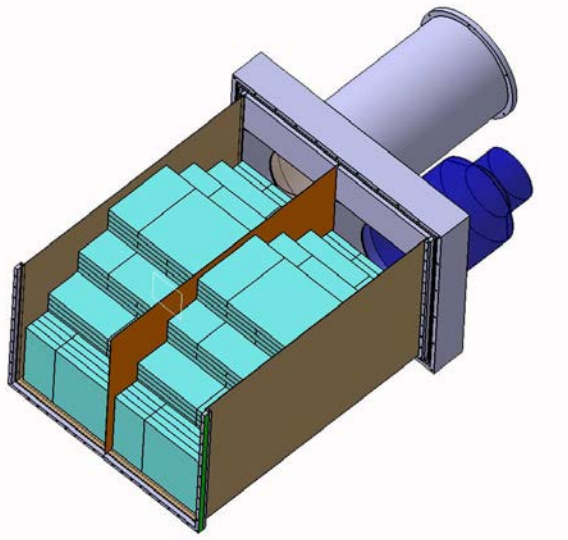

Figure 2.11: *Exploded view of the $n = 1.015$ aerogel counter showing the pyramidal design.*

References

[1] B. Adeva *et al.* (DIRAC Collaboration), Phys. Lett. **B 619** (2005) 50
[2] J. Schweizer, Eur. Phys. J **C 36** (2004) 483; Phys. Lett. **B 587** (2004) 33
[3] P. Estabrooks *et al.*, Nucl. Phys. **B 133** (1978) 490
[4] P. Büttiker, S. Descotes-Genon, B. Moussallam, Eur. Phys. J. **C 33** (2004) 409
[5] G. Colangelo, J. Gasser and H. Leutwyler, Nucl. Phys. **B 603** (2001) 125
and references therein
[6] S. Pislak *et al.*, Phys. Rev. **D 67** (2003) 072004
[7] V. Bernard *et al.*, Nucl. Phys. **B 357** (1991) 129
[8] M. Ablikim et *et al.* (BES Collaboration), Phys. Lett. **B 633** (2006) 681
[9] For a review see C. Amsler and N. Törnqvist, Phys. Rep. **389** (2004) 61
[10] B. Adeva *et al.*, Nucl. Instr. and Meth. in Phys. Research **A 515** (2003) 467
[11] B. Adeva *et al.*, Add. to DIRAC proposal, CERN - SPSC - 2004 - 009
[12] A. R. Buziatev *et al.*, Nucl. Instr. Meth. in Phys. Research **A 433** (1999) 396

3 Towards a dark matter experiment

C. Amsler, V. Boccone, A. Büchler‡, A. Knecht‡, C. Regenfus, and J. Rochet

‡ Diploma student

In collaboration with:
CIEMAT, ETHZ, Soltan Institute (Warsaw), Universities of Granada and Sheffield

(ArDM Collaboration).

3.1 Introduction

The search for dark matter is one of the most pressing activities in particle physics. Dark matter is probably made of Weakly Interacting Massive Particles (WIMP) which are stable particles trapped in the gravitational fields of galaxies. The favored candidate for WIMPs is the lightest supersymmetric (SUSY) particle, the neutralino with a mass of at least 40 GeV, according to LEP searches. The direct detection of WIMPs involves scattering on target nuclei with recoil energies in the range 1 - 100 keV. The cross-sections are tiny but rate predictions are model dependent, and therefore uncertain by several orders of magnitude. They depend e.g. on the nuclear target (atomic number, spin, form factors) and the type of detector used (energy threshold, resolution, signal discrimination). The search for WIMPS is hence experiment driven. The experimental upper limit for the cross-section of WIMPS with nucleons is about 10^{-6} pb.

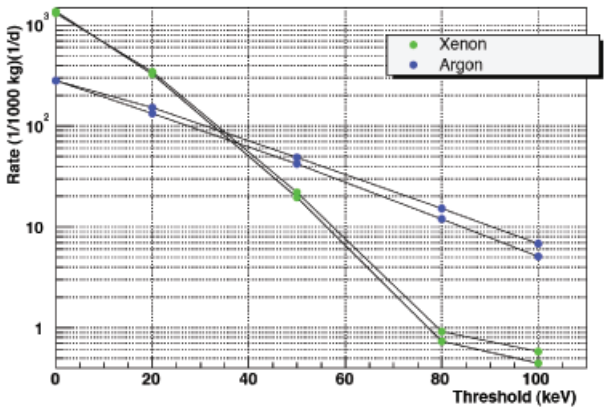

Figure 3.1: *Expected daily WIMP detection rate for a 1 ton detector as a function of threshold for xenon and argon, assuming a mass of 100 GeV and a cross section of 10^{-6} pb. The steeper curve is for xenon.*

Noble liquid detectors such as xenon or argon could act as target for WIMP detection. They have high scintillation and ionization yields because of their relatively low ionization potentials. Ionisation electrons *and* scintillation light may be detected [1]. Argon is less sensitive to the threshold of the nuclear recoil energy than xenon, because of form factors, and is also much cheaper. Also, recoil energy spectra in xenon and argon are quite different (fig. 3.1). These liquids are therefore complementary in providing a crosscheck once a WIMP signal has been found.

3.2 The liquid argon detector

We describe here R &D developments for an experiment that could possibly reach a cross-section of 10^{-10} pb. The detector (fig. 3.2) would contain 1 ton of liquid argon. It exploits the ratio of scintillation to ionisation in argon and the scintillation time discrimination between nuclear and electron recoils. With a nuclear recoil energy threshold of say 30 keV, a WIMP-nucleon cross-section of 10^{-6} pb would yield 100 events per day per ton. Therefore, a 1 ton argon detector could improve

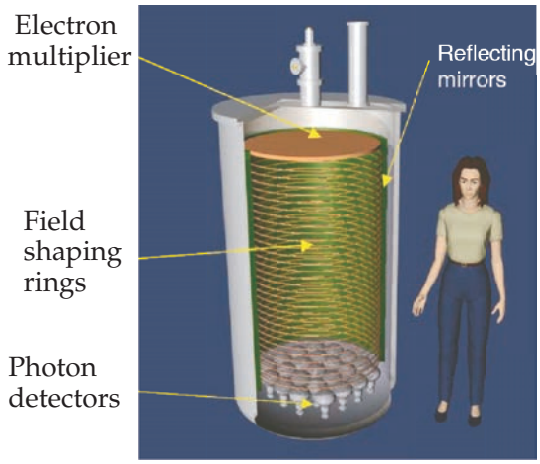

Figure 3.2: *Artist's view of the 1 ton ArDM liquid argon detector to search for WIMPS.*

significantly on the upper limits, provided that the threshold of 30 keV and sufficient background rejection can be achieved. A drawback of natural argon liquefied from the atmosphere is namely the radioactive β-emitter ^{39}Ar. Its activity in atmospheric argon has been measured to be about 1 Bq/kg [2]. It therefore induces a background rate of about 1 kHz in a 1 ton detector. The first milestone in the design of an experiment is therefore the optimization of the light detection from nuclear recoils and and the rejection of the γ and β background. Figure 3.3 shows the two mechanisms leading to the emission of 128 nm light in argon.

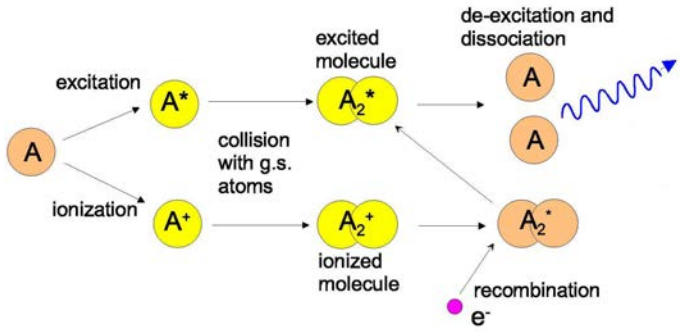

Figure 3.3: *The two mechanisms leading to the emission of 128 nm photons are excitation* $Ar^* + Ar \rightarrow Ar_2^* \rightarrow Ar + Ar + \gamma$ *and ionisation* $Ar^+ + Ar \rightarrow Ar_2^+ + e^- \rightarrow Ar_2^* \rightarrow Ar + Ar + \gamma$. *The energy required to generate a photon is 68 eV.*

The concept of WIMP detection in argon is shown in fig. 3.4. Primary scintillation light from argon and secondary charge signals are read independently. Following an ionizing event, ionization charges drift towards the top of the detector where they are extracted from the liquid to the gas phase. An electron multiplier system then amplifies the electrons to produce a detectable signal. The ratio of the scintillation to the ionization yields is extremely high for WIMP events, due to quenching. Very high drift fields up to 5 kV/cm must be reached to detect an ionization signal from highly quenched nuclear recoils.

Because background discrimination requires a high ratio of scintillation to ionization yields, the VUV scintillation light needs to be detected efficiently. This is the main task and responsibility of the Zurich group. We are also investigating alternative schemes to photomultipliers, such as wavelength shifters read out by avalanche photodiodes (APD).

3.3 Light collection

Monte Carlo simulations suggest that a light collection efficiency of at least 5% for 128 nm photons will be required to suppress the background from ^{39}Ar β-decay. However, VUV photons are absorbed by most materials, with few exceptions such as MgF_2 and LiF. A large area coverage using phototubes

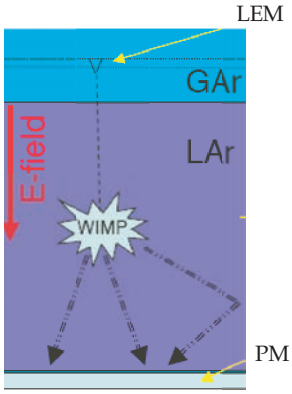

Figure 3.4: *Principle of WIMP detection in liquid argon (LAR). WIMPs lead to a high ratio of primary scintillation light detected by the photo-multipliers (PM) to charge collected by the electron multiplier (LEM) in gaseous argon (GAR).*

with MgF_2 windows is excluded for cost reasons. Also, the operation of phototubes at cryogenic temperatures requires photocathodes with a metallic underlayer to prevent electrical charge-up.

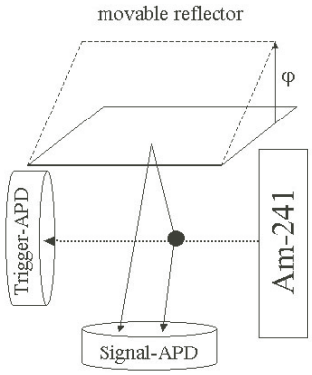

Figure 3.5: *Setup used to measure the reflectivity of various coated mirrors.*

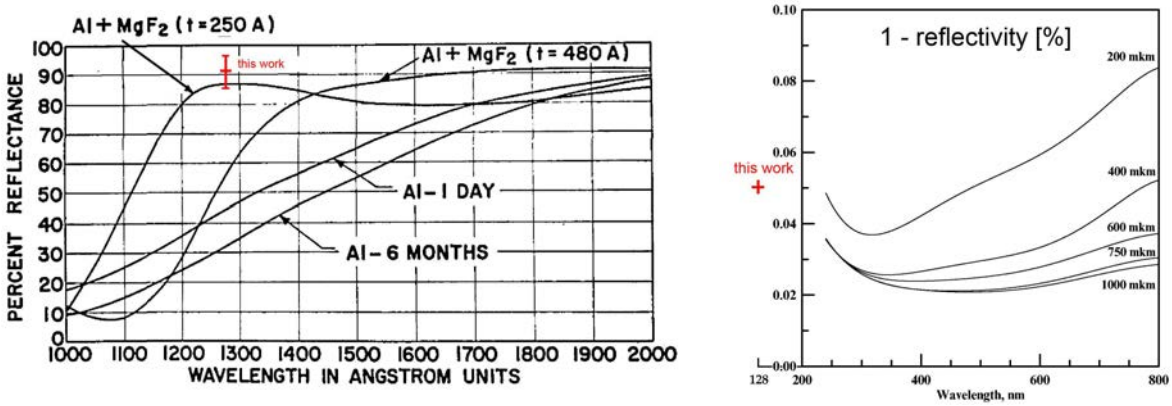

Figure 3.6: *Reflectivity of Al + MgF_2 (left, from ref. [4]) and Tetratex (right, from ref. [5]), compared to our own measurements.*

However, 128 nm light can be reflected or wavelength shifted. We have therefore investigated aluminized mylar foils with MgF_2 coating and Tetratex (porous teflon) foils as specular or diffuse VUV-mirrors [3]. The reflecting material is mounted on a rotating frame in the test box immersed in clean gaseous argon at NTP (fig. 3.5). The gas atoms are excited by α- particles yielding 68 eV/ emitted photon and leading to tracks of typically 5 cm length. An APD is used as the trigger. Direct and reflected photons are measured by another large area APD (15 mm in diameter) with a wide spectral range. The reflection coefficient is derived from the measurement by Monte Carlo simulation

of the acceptance, as a function of mirror angle φ. These results are shown in fig. 3.6, superimposed to measurements from literature. For Al + MgF_2 we obtain a reflectivity of 91.5% and for Tetratex 95%. The high reflectivity of Tetratex is probably due to the fluorescence of teflon in the yellow region.

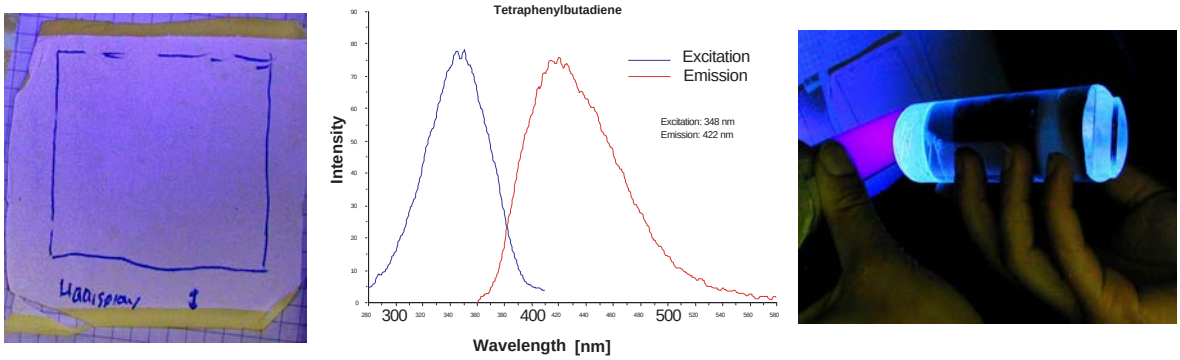

Figure 3.7: *Reflection of UV light on teflon coated with TPB (left) and emitted light (right). The middle plot shows the absorption and emission spectra of TPB.*

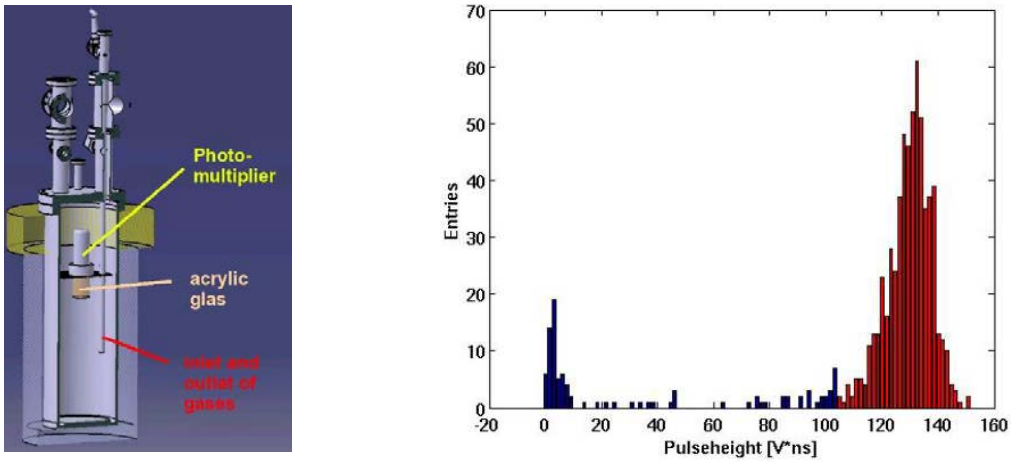

Figure 3.8: *Left: Vacuum chamber. Right: Intensity distribution of the 128 nm light measured in gaseous argon.*

Large area APDs (from Advanced Photonics) with very thin entrance windows read the 128 nm light. Their quantum efficieny is about 60% at 128 nm [6]. However, their small active area require a method for light concentration. We have therefore investigated wavelength shifters bound to light guides with filling materials such as polystyrene [7]. Preliminary tests with Tetratex foils or acrylic glass coated with wavelength shifters give promising results. Figure 3.7 shows two samples illuminated with 250 nm UV light. The white-blueish centre of the Tetratex sample (left) was coated with tetraphenylbutadiene (TPB) dissolved in chloroform before being sprayed on the teflon tissue. The absorption maximum of TPB is around 340 nm, its emission maximum around 420 nm (middle plot). The yellow fluorescence of the uncoated teflon can be clearly seen around the borders. Figure 3.7 (right) shows a TPB/polystyrene mixture applied to one end of a plexiglas cylinder, which demonstrates trapping of the emitted light at 420 nm from TPB.

To test functionality and measure light yields, decay times, outgasing and other properties, we have built a 7 ℓ vacuum chamber which can be filled with gaseous or liquid argon (fig. 3.8). The

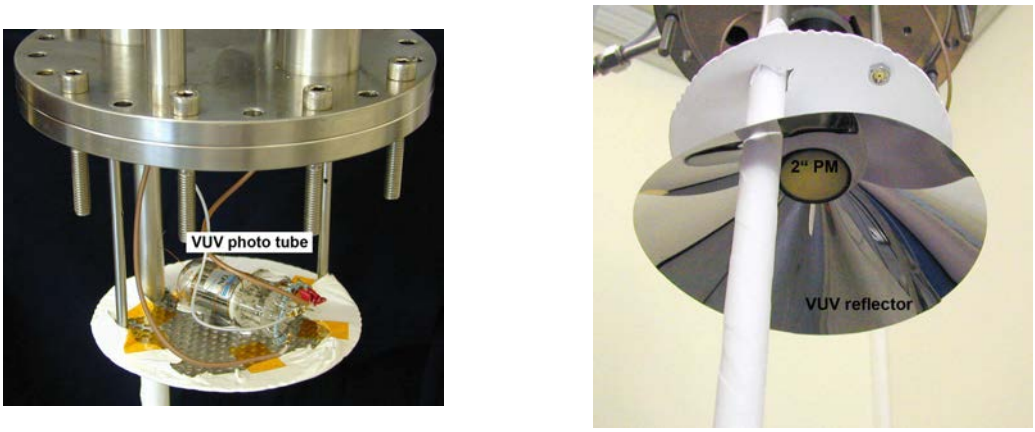

Figure 3.9: *Left: Vacuum chamber with VUV tube. Right: Bialkali tube with reflector.*

chamber will also be used to search for the ^{39}Ar signal. A gas purification system filters out residual water or oxygen traces, both being strong UV absorbers. The gas composition is monitored by a quadrupole mass spectrometer with high sensitivity (10^{-10}) connected through a dosing valve. Figure 3.9 (left) shows the top flange holding a small VUV phototube (1 cm^2 Cs-Te photocathode) with MgF_2 window. This device has a narrow spectral response (115-320 nm) and a well known quantum efficency ($\sim$ 25%) and is therefore mainly used for calibration. Figure 3.9 (right) shows a standard bialkali photomultiplier (2", 300-600 nm) mounted on the flange for the first spectroscopical measurements.

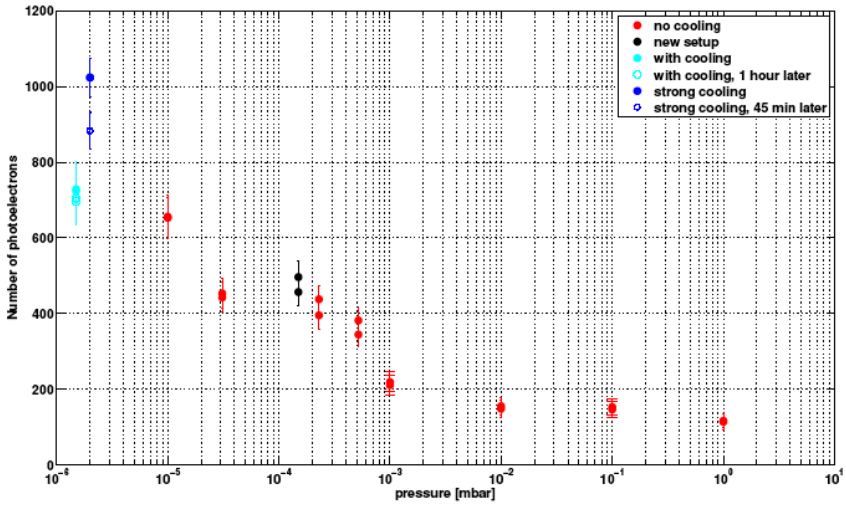

Figure 3.10: *Number of photoelectrons as a function of residual partial air pressure measured for different experimental conditions (from ref. [8]).*

Figure 3.8 (right) shows an intensity spectrum from 5.3 MeV α's emitted by a ^{210}Po source in argon gas at NTP. With a total coverage of the inner wall with TPB coated Tetratex we could obtain 885 photoelectrons (p.e.), corresponding to a detection efficiency of roughly 1%, which is already encouraging for a large detector. This setup should be able to detect the ^{39}Ar decays with a mean energy deposit of 218 keV (corresponding to 30 p.e.).

However, as fig. 3.10 shows, the number of photoelectrons depends crucially on the purity of argon. The data sample at a partial air pressure of 2×10^{-6} mbar was selected to analyze the time

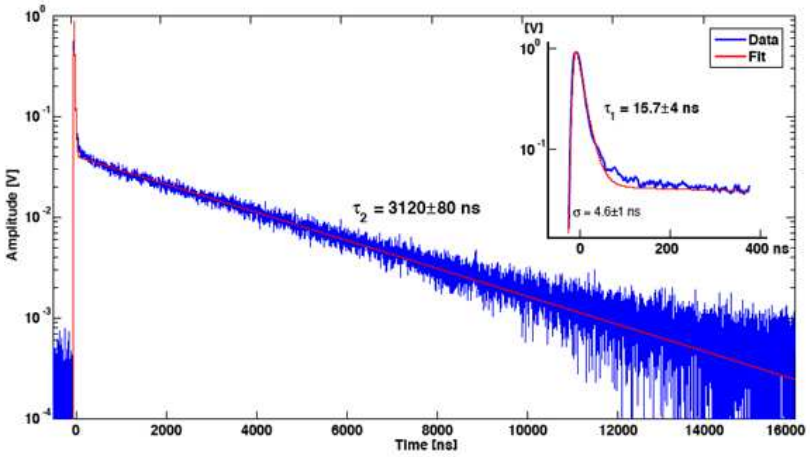

Figure 3.11: *Light intensity as a function of time showing the fast and slow components of scintillating argon (from ref. [8])*.

evolution of the light output in gaseous argon. The signal amplitude is shown as a function of time in fig. 3.11. One clearly observes two components which correspond to the decay of the singlet and triplet molecular states. The data were fitted by two exponential functions convoluted with a Gaussian to describe the time resolution. The fast component has a mean life of 15.7 $\pm$ 4.0 ns, the slow component a mean life of 3.12 $\pm$ 0.08 μs. The latter agrees with the published value 3.2 $\pm$ 0.3 s [9].

These developments will be pursued in 2006 with liquid argon. We will then investigate the performance of APDs using focussing Winston cones. Assuming that enough light can be detected we will then formally propose a dark matter experiment e.g. in the underground Canfranc Laboratory in Spain. We have already expressed our interests to the corresponding Scientific Committee.

References

[1] P. Cennini *et al.*, Nucl. Instr. Methods in Phys. Research **A 432** (1999) 240
[2] P. Benetti *et al.* (WARP Collaboration), preprint astro-ph/0603131 (2006)
[3] A. Knecht, Diploma Thesis, ETHZ, 2005
[4] L. Canfield *et al.*, Applied Optics **5** (1966) 45
[5] A. Buzykaev *et al.*, Nucl. Instr. Methods in Phys. Research **A 379** (1996) 453
[6] R. Chandrasekharan, M. Messina, and A. Rubbia, Nucl. Instr. Methods in Phys. Research **A 546** (2005) 426
[7] G. Eigen, E. Lorenz, Nucl. Instr. Methods **166** (1979) 165
[8] A. Büchler, Bachelor Thesis, Universität Zürich, 2006
[9] J.W. Keto *et al.*, Phys. Rev. Lett. **33** (1974) 1365

4 Publications

Articles

- Final results on the neutrino magnetic moment from the MUNU experiment
  Z. Daraktchieva et al. (MUNU Collaboration)
  Phys. Lett. **B 615** (2005) 153

- Vertex reconstruction in CMS
  E. Chabanat et al.
  Nucl. Instr. Meth. in Phys. Research **A 549** (2005) 188

- The effect of highly ionising particles on the CMS silicon strip tracker
  W. Adam et al.
  Nucl. Instr. Meth. in Phys. Research **A 543** (2005) 463

- Simulation of Heavily Irradiated Silicon Pixel Sensors and Comparison
  With Test Beam Measurements
  V. Chiochia et al.
  IEEE Trans. Nucl. Sci. **52** (2005) 1067

- Fluence dependence of charge collection of irradiated pixel sensors
  T. Rohe et al.
  Nucl. Instr. Meth. in Phys. Research **A 552** (2005) 232

- Study of the $B_s^0 \to (J/\psi)\phi \to \mu^+\mu^- K^+ K^-$ Decay with the CMS Detector at LHC
  K. Prokofiev
  PhD Thesis, Universität Zürich, 2005

- Results from Athena
  A. Rotondi et al. (ATHENA Collaboration)
  AIP Conference Proceedings **796** (2005) 285

- Cold - Antimatter Physics
  M. Amoretti et al. (ATHENA Collaboration)
  XLIII Int. Meeting on Nuclear Physics, Bormio, 2005
  Ric. Sci. **124** (2005) 25, prep. hep-ex/0503034

- Detection of Antihydrogen Annihilations with a Si-Micro-Strip and pure CsI Detector
  I. Johnson et al. (ATHENA Collaboration)
  Proc. of the 8th ICATPP Conf. on Astroparticle, Particle, Space Physics, Detectors and Medical Physics Applications
  World Scientific (2004) 473, prep. physics/0401034

- ATHENA - First Production of Cold Antihydrogen and Beyond
  A. Kellerbauer et al. (ATHENA Collaboration)
  Proc. of the Third Meeting on CPT and Lorentz Symmetry, Bloomington, USA
  World Scientific (2005) 38, prep. hep-ex/0409045

- Production of Cold Antihydrogen with ATHENA for Fundamental Studies
  A. Kellerbauer et al. (ATHENA Collaboration)
  Proc. of the XXXIXth Rencontres de Moriond 2004
  Gioi Publishers (Hanoi, Ed. J. Tran Thanh Van 2005) 385, prep. hep-ex/0406074

- A Gaussian-sum filter for vertex reconstruction
  T. Speer and R. Frühwirth
  Proc. of the 2004 Conf. for Computing in High-Energy and Nuclear Physics (CHEP 04), Interlaken, 2004
  CERN Yellow Report 2005-002

- A kinematic fit and a decay chain reconstruction library
  K. Prokofiev and T. Speer
  Proc. of the 2004 Conf. for Computing in High-Energy and Nuclear Physics (CHEP 04), Interlaken, 2004
  CERN Yellow Report 2005-002

- Design and performance of the CMS Pixel Detector Barrel Modules
  C. Hörmann
  Proc. 11 Workshop on Electronics for LHC and future Experiments, Heidelberg
  CERN-LHCC 2005-038 (2005)

Articles in press

- Study of $K\bar{K}$ resonances in $\bar{p}p \to K^+K^-\pi^0$ at 900 and 1640 MeV/c
  C. Amsler et al. (CRYSTAL BARREL Collaboration)
  Phys. Lett. **B**

- CMS Physics technical design report volume I : Software and detector performance
  E. Alagöz et al.
  CMS - TDR - 08, CERN-LHCC-2006-001

- A Gaussian sum - Filter for the Vertex Reconstruction
  T. Speer and R. Frühwirth
  Comp. Phys. Comm.

- A double junction model of irradiated silicon pixel sensors for LHC
  V. Chiochia et al.
  Proc. 10th Eur. Symp. on Semiconductor Detectors: New Developments in Radiation Detectors, Wildbad Kreuth, Germany, 2005.
  Prep. physics/0506228, Nucl. Instr. Meth. in Phys. Research **A**

- Track reconstruction at the CMS experiment
  T. Speer et al.
  Proc. of the X Int. Workshop on Advanced Computing and Analysis Techniques in Physics Research (ACAT 05), DESY Zeuthen, Germany, 2005
  Nucl. Instr. Meth. in Phys. Research **A**

- Simulation and hit reconstruction of irradiated pixel sensors for the CMS experiment
  E. Alagöz, V. Chiochia, M. Swartz
  Proc. of the Workshop on Tracking in High Multiplicity Environments (TIME 2005), Zurich
  Prep. physics/0512027, Nucl. Instr. Meth. in Phys. Research **A**

- Sensor simulation and position calibration for the CMS pixel detector
  V. Chiochia
  Proc. of Vertex 2005 - 14th Int. Workshop on Vertex detectors,
  Chuzenji Lake, Nikko, Japan, 2005
  Prep. physics/0603192, Nucl. Instr. Meth. in Phys. Research **A**

- Extraction of electric field in heavily irradiated silicon pixel sensors
  A. Dorokhov et al.
  Proc. Vertex 2004 Conf., Como, 2004
  Prep. physics/0412036, Nucl. Instr. Meth. in Phys. Research **A**

- Study of the $B_s \to J/\psi\,\phi$ Channel with CMS
  V. Ciulli et al.
  Proc. of the X Int. Conf. on B - Physics at Hadron Machines, Assisi, Italy, 2005
  Nucl. Phys. **B**

- Robust Vertex Fitters
  T. Speer et al.
  Proc. of the Workshop on Tracking in High Multiplicity Environments (TIME 2005), Zurich
  Nucl. Instr. Meth. in Phys. Research **A**

- Observation, modeling and temperature dependence of doubly peaked electric fields in irradiated silicon pixel sensors
  M. Swartz et al.
  Proc. at the Pixel 2005 Conf., Bonn, 2005
  Prep. physics/0510040, Nucl. Instr. Meth. in Phys. Research **A**

- The Control and Readout Systems of the CMS Pixel Barrel Detector
  D. Kotlinski et al.
  Proc. at the Pixel 2005 Conf., Bonn, 2005
  Nucl. Instr. Meth. in Phys. Research **A**

- Assembly of the CMS Pixel Barrel Modules
  S. König et al.
  Proc. at the Pixel 2005 Conf., Bonn, 2005
  Nucl. Instr. Meth. in Phys. Research **A**

- Design and Performance of the CMS Pixel Detector Readout Chip
  H. Chr. Kästli et al.
  Proc. at the Pixel 2005 Conf., Bonn, 2005
  Nucl. Instr. Meth. in Phys. Research **A**

- Progress with Cold Antihydrogen
  M. Amoretti et al. (ATHENA Collaboration)
  Proc. of XIII Int. Workshop on Positron and Positronium Physics (P0S05)
  Nucl. Instr. Meth. in Phys. Research **B**

Invited Lectures

- E. Alagöz
  Contributed paper, Jahrestagung der SPG, Lausanne, 14 February 2006
  "Hit reconstruction at CMS from irradiated silicon pixels"

- Y. Allkofer
  Seminar, Budker Institute of Nuclear Physics, Novosibirsk, 14 September 2005
  "The lifetime measurement of $\pi^{\pm}K^{\mp}$ atoms with DIRAC"

- Y. Allkofer
  Contributed paper, Jahrestagung der SPG, Lausanne, 14 February 2006
  "Large area Čerenkov counter for kaon - proton separation between 4 and 8 GeV/c"

- C. Amsler
  Contributed talk, CHIPP plenary meeting, Paul Scherrer Institute, 28 September 2005
  "$K\pi$ atoms with DIRAC"

- C. Amsler
  Invited talk, CHIPP plenary meeting, Paul Scherrer Institute, 28 September 2005
  "Report of NuPECC activities"

- V. Chiochia
  Invited talk, ESSD - 10th Eur. Symp. on semiconductor detectors, Wildbald, Kreuth, Germany, 12 June 2005
  "Charge collection in irradiated pixel sensors : beam test measurements and simulation"

- V. Chiochia
  Invited talk, CHIPP plenary meeting, Paul Scherrer Institute, 28 September 2005
  "The compact muon solenoid : Status of preparation"

- V. Chiochia
  Invited talk, Workshop on Tracking in High Multiplicity
  Environments (TIME 05), Zurich, 7 October 2005
  "Charge collection in irradiated pixel sensors : beam test and simulation"

- V. Chiochia
  14th Int. Workshop on Vertex Detectors (VERTEX 2005), Nikko, Japan, 9 November 2005
  "CMS pixel simulation"

- V. Chiochia
  Seminar, DESY - Hamburg, 7 March 2006
  "Silicon tracking detectors for the LHC experiments"

- V. Chiochia
  Seminar, DESY - Zeuthen, 8 March 2006
  "Silicon tracking detectors for the LHC experiments"

- C. Hörmann
  Invited talk,11th Workshop on Electronics for LHC and Future Experiments, Heidelberg, 15 September 2005
  "Performance of CMS pixel detector barrel modules"

- K. Prokofiev
  Invited talk to the X Int. Conf. on B-Physics at Hadron Machines, Assisi, 22 June 2005
  "Study of the $B_s \to J/\psi\,\phi$ Channel with CMS"

- T. Speer
  Invited talk to the X International Workshop on Advanced Computing and Analysis Techniques in Physics Research, Berlin, Germany, 25 May 2005
  "Track reconstruction in the CMS tracker"

- T. Speer
  Invited talk, Workshop on Tracking in High Multiplicity Environments (TIME 05), Zurich, 5 October 2005
  "Adaptative filter and gaussian sum filter for vertex reconstruction"

- T. Speer
  Invited talk, Proc. of Flavour Workshop in the Era of the LHC, CERN, 9 November 2005
  "Search for the decay B_s to $\mu^+\mu^-$ at CMS"

- L. Wilke
  Contributed talk, DPG - Tagung, Dortmund, 28 March 2006
  "Extracting $\Delta\Gamma$ in the B_s system from angular distributions of the $B_s \to J/\psi\phi$ decay with the CMS detector"

ATHENA Collaboration (2005):
M. Amoretti, C. Amsler, G. Bonomi, P. Bowe, C. Canali, C. Carraro, C. L. Cesar, M. Charlton, M. Doser, A. Fontana, M. C. Fujiwara, R. Funakoshi, P. Genova, J. S. Hangst, R. S. Hayano, A. Kellerbauer, L. V. Joergensen, I. Johnson, V. Lagomarsino, R. Landua, E. Lodi Rizzini, M. Macri, N. Madsen, G. Manuzio, D. Mitchard, P. Montagna, H. Pruys, C. Regenfus, J. Rochet, A. Rotondi, G. Testera, A. Variola, D. P. van der Werf, Y. Yamazaki, N. Zurlo

MUNU Collaboration (2005):
C. Amsler, M. Avenier, C. Broggini, J. Busto, C. Cerna, Z. Daraktchieva, F. Juget, D.H. Koang, J. Lamblin, D. Lebrun, O. Link, G. Puglierin, A. Stutz, A. Tadsen, J.-L. Vuilleumier, V. Zacek

CRYSTAL BARREL Collaboration (2006):
C. Amsler, C. A. Baker, B. M. Barnett, C. J. Batty, M. Benayoun, P. Blüm, K. Braune, V. Credé, K. M. Crowe, M. Doser, W. Dünnweber, D. Engelhardt, M. A. Faessler, R. P. Haddock, F. H. Heinsius, N. P. Hessey, P. Hidas, D. Jamnik, H. Kalinowsky, P. Kammel, J. Kisiel, E. Klempt, H. Koch, M. Kunze, U. Kurilla, R. Landua, H. Matthäy, C. A. Meyer, F. Meyer-Wildhagen, R. Ouared, K. Peters, B. Pick, M. Ratajczak, C. Regenfus, U. Strohbusch, M. Suffert, U. Thoma, I. Uman, S. Wallis-Plachner, D. Walther, U. Wiedner, B. S. Zou, Č. Zupančič

DIRAC Collaboration (2006):
B. Adeva, L. Afanas'ev, Y. Allkofer, C. Amsler, D. Bartos, A. Benelli, V. Brekhovskikh, A. Caraghe-orgheopol, T. Cechak, M. Chiba, S. Constantinescu, C.O. Curceanu, C. Detraz, D. Dreossi, D. Drijard, A. Dudarev, I. Evangelou, J. L. Fungueirino Pazos, J. Gerndt, P. Gianotti, G. Giolu, O. Gorchakov, K. Gritsay, C. Guaraldo, M. Hansroul, S. Horikawa, M. Iliescu, V. Karpukhin, J. Kluson, M. Kobayashi, P. Kokkas, V. Komarov, L. Kruglova, V. Kruglov, A. Kulikov, A. Kuptsov, K. I. Kuroda, A. Lamberto, A. Lanaro, V. Lapchine, R. Lednicky, P. Levi Sandri, L. Lopez Aguera, V. Lucherini, N. Manthos, C. Marinas Pardo, L. Nemenov, M. Nikitin, K. Okada, V. Ol'shevskiy, M. Pentia, A. Penzo, M. Plo, T.C. Ponta, Z. Pustylnik, G.F. Rappazzo, J. Rochet, A. Romero Vidal, J. J. Saborido Silva, J. Schacher, F. Takeutchi, A. Tarasov, L. Tauscher, F. A. Triantis, T. Trojek, S. Trusov, J. Smolik, S. Sugimoto, A. Ryazantsev, V. Rykalin, O. Vazquez Doce, T. Vrba, V. Yaz'kov, M. Zhabitskiy, P. Zrelov